CHIN. PHYS. LETT. Vol. 31, No. 7 (2014) 075202

Quasi-Monoenergetic Electron Beam Generation from Nanothickness Solid Foils Irradiated by Circular-Polarization Laser Pulses *

SU Heng-Yi(苏恒毅)[1], HUANG Yong-Sheng(黄永盛)[1**], WANG Nai-Yan(王乃彦)[1], TANG Xiu-Zhang(汤秀章)[1], LU Wei(鲁巍)[2]

[1]*High Power Excimer Laser Laboratory, China Institute of Atomic Energy, Beijing 102413*
[2]*Department of Engineering Physics, Tsinghua University, Beijing 100084*

(Received 5 March 2014)

Ultrashort 10^{22}–10^{24} W/cm^2 laser pulses will offer the possibility of producing monoenergetic electron beams in the GeV–TeV level in the future. A laser-electron acceleration scheme is proposed by the interaction between a thin solid foil and an ultra-intense laser pulse for $a_0 \geq 800\sigma_0$, where a_0 is the normalized laser field and σ_0 is the normalized plasma surface density. The energy of the electrons as a function of time can be described by a simple model which indicates that an exponential relationship exists between the energy and the normalized time τ. A quasi-monoenergetic high density electron beam with 1.3 GeV energy and a 2.2% energy spread has been predicted for $a_0 = 223.5$ by particle-in-cell simulations. Characteristics of the ultra-high density electron layer formed in the early period of the acceleration are discussed.

PACS: 52.38.Kd, 41.75.Jv, 52.65.Rr, 52.35.Py DOI: 10.1088/0256-307X/31/7/075202

With the development of ultrashort high intensity laser technology, great advances in the laser-plasma-based acceleration have been made in the past few decades. High energy monoenergetic electron beams produced by laser-plasma-based acceleration are promising for broad applications such as radiotherapy in medicine and biology,[1,2] material science,[3] terahertz radiation generation,[4,5] and bright ultrashort x-ray pulses generation.[6] In the past few decades, several acceleration mechanisms have been established and widely researched, such as the laser wakefield acceleration (LWFA),[7–10] the plasma beat wave acceleration (PBWA),[11,12] and the multiple laser pulses acceleration.[13] Recently, an all-optical cascaded laser wakefield accelerator by using ionization-induced injection has produced near-GeV electron beams.[14] However, in the bubble or blowout regime, to optimize the wakefield generation and to obtain high quality electron beams, $\lambda_p/2 \sim c\tau_0$ should be satisfied,[10] which requires $n_{e0} < n_c$, where λ_p is the plasma wavelength, c is the speed of light, τ_0 is the laser pulse duration, n_{e0} is the initial electron density, and n_c is the critical density. Therefore, the density of targets is restricted to being under-dense so that the number of accelerated electrons is limited as well as the acceleration length without using capillaries to channel the laser pulse. The intensity of laser pulses will be higher than 10^{22} W/cm^2 in the near future, e.g., the extreme light infrastructure (ELI) will be constructed soon.[15] However, even such a high intensity laser pulse is incident on the target, the energy of the electrons is limited if $n_{e0} \approx n_c$ with few-cycle laser pulses. Experimental results and numerical simulations indicate that a plasma density less than 10^{19} cm^{-3} is optimal to produce GeV electron beams.[16,17] To date, laser-plasma accelerators have also reached the GeV level(1–2 GeV).[14,18–20]

On the other hand, the laser-plasma acceleration presents new opportunities to discover and examine new phenomena in the parametric region $a_0 \gg \sigma_0 = \hat{n}_e\hat{l}_e$, where $a_0 = eE_l/m_e\omega c$, E_l is the peak electric field of the laser pulse, ω is the laser frequency, e is the elementary charge, m_e is the electron mass, the normalized electron density $\hat{n}_e = n_{e0}/n_c, \hat{l}_e = l_e/\lambda$, λ is the laser wave length, and l_e is the thickness of the target. In this case, laser-overdense-plasma interaction which has been used for proton acceleration such as target normal sheath acceleration (TNSA)[21] and radiation pressure acceleration (RPA)[22] may present good prospects. High energy electron beams (600 MeV) have been predicted from the laser-overdense-plasma interaction via the laser ponderomotive force acceleration mechanism for $a_0 = 60.4$ and $\hat{n}_e\hat{l}_e = 0.1$, while the energy spread is not smaller than 10%.[23] The energy spread is defined as $\Delta E/E_{peak}$, where E_{peak} is the peak energy of the electron energy spectrum, and ΔE is the full width at half maximum (FWHM) of the electron energy spectrum. In this parametric region, a relativistic electron mirror (REM) appears and high energy electron bunches can be obtained quickly.[24,25] Previously, quasi-monoenergetic electron beams were generated from a femtosecond prepulse-exploded foil,[26] via a high-contrast femtosecond pulse interacting with a solid foil[27] and from laser-solid interactions at 0.5 kHz.[28] Electron beams with MeV energy and ∼20% energy spread were obtained.

In this Letter, we propose to use a nano-thickness foil irradiated by a circularly polarized (CP) laser to generate high quality electron beams for $a_0 \geq 800\sigma_0 = \hat{n}_e\hat{l}_e$. Quasi-monoenergetic electron beams with 1.3 GeV energy and 2.2% energy spread have been obtained easily without external laser guiding or specific injection in comparison with LWFA. By opti-

*Supported by the National Basic Research Program of China under Grant No 2011CB808104, and the National Natural Science Foundation of China under Grant Nos 11105233 and 11105234.
**Corresponding author. Email: huang_y_s@163.com
© 2014 Chinese Physical Society and IOP Publishing Ltd

mizing the parameters of laser pulses and source foils, the REM can maintain its shape until about 1 ps. To show the acceleration mechanism clearly including the effects of transverse expansion, a two-dimensional PIC simulation has been performed and a simple model has been used to fit the simulation results.

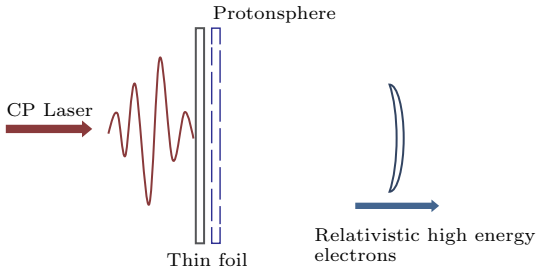


Fig. 1. (Color online) The schematic diagram of the new electron acceleration scheme induced by an intense circularly polarized laser pulse incident on a thin foil. During the whole simulation time duration, the ions only move a very short distance (about 2 μm) compared to the electrons in the laser pulse propagating direction (as the blue dotted rectangle frame shows). On the other hand, the electrons are accelerated to relativistic energy and move with the laser pulse.

Figure 1 shows the schematic diagram of the electron acceleration scheme induced by an intense laser pulse incident on a thin foil. In the duration of the interaction, electrons obtain relativistic energy in an ultrashort time duration. For instance, the electrons are accelerated to about 106 MeV only in 3.6 fs with a 21 fs CP laser pulse ($a_0 = 223.5$) irradiating on a 10 nm foil ($\hat{n}_e\hat{l}_e \simeq 0.4$) in the following PIC simulation. Electrons in the leading edge of the laser pulse are accelerated efficiently with a slight energy spread and angle divergence. The laser pulse is like a snow plow. The electrons are compressed into a high-density ultra-thin layer while the ions just move a very short distance (about 2 μm) compared to the electrons. In this case, the normalized charge separation field $\epsilon = k_L l_e n_{e0}/n_c$ is much smaller than the amplitude of the laser field a_0,[29] and the electrons are accelerated by ponderomotive force $F_p = -m_e c^2 \nabla\gamma$ and radiation pressure into the relativistic regime, where γ is the electron relativistic factor and $k_L = 2\pi/\lambda$.

To demonstrate the generation of the high-quality electron beams, we performed a 2D PIC simulation by OSIRIS code.[30] A single intense laser pulse with the amplitude $a_0 = 223.5$ ($a_0 \geq 800\sigma_0$), the focus radius of $r_0 = 1$ μm and a Gaussian transverse profile was chosen. It had a 'flat-top' temporal profile of 21 fs with a very sharp rising edge and propagated along the $+x$-direction with the wavelength of 800 nm. To reduce the Coulomb expansion of the electrons, one needs to decrease σ_0. Therefore, we used nanofoils positioned at $x_0 = 84.0127$ μm with a fixed thickness of 10 nm while different initial densities such as $n_{e0} = n_{i0} = 5n_c$, $n_{e0} = n_{i0} = 15n_c$, $n_{e0} = n_{i0} = 25n_c$, and $n_{e0} = n_{i0} = 30n_c$, respectively. Here n_{i0} is the initial ion density and the ions (protons) mass m_i satisfies $m_i = 1836m_e$. The ions and electrons were evenly mixed and distributed in the foils. The ions are mobile during the whole simulation time. The incident laser pulse arrived at the foil surface as long as $t > 0$ and the simulation time was 864.77 fs. An initial simulation area of 535.42 μm^2 was used, subdivided into a grid of 120000000 cells (150000 cells in the x-direction and 800 cells in the y-direction). The mesh size is 0.56×7.96 nm^2 and the minimum size that the mesh can resolve is 0.56 nm in the x-direction. Therefore, the grid space can be small enough to resolve the laser pulse bandwidth (800 nm), the laser focal spot (1 μm) and the thickness of the foil (10 nm). During the interaction, the diagnostic area moved at the speed of light to guarantee that the electrons would not escape from it. The effect of pre-plasma or laser contrast was not considered.

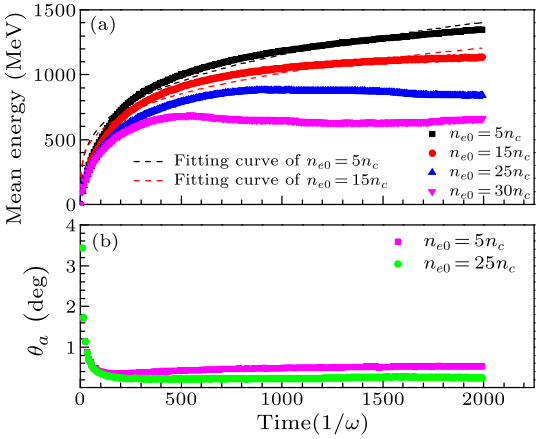


Fig. 2. (Color online) Simulation results by 2D OSIRIS: the average energy and the average angle divergence as a function of time, where the curves with different colors in every plot denote the source foils with different initial electron densities, the dashed lines in (a) are fitting curves given by a simple equation $E_a = a\tau^b$, where a and b are constants and τ is normalized by laser frequency ω. The black dashed line (only fitting the black data points) and red dashed line (only fitting the red data points) represent $E_a \propto \tau^{0.28}$ and $E_a \propto \tau^{0.25}$, respectively. Only the electrons within the laser pulse leading edge are counted.

For the purpose of showing the complete picture of the simulation results, the temporal evolution of the parameters such as average energy and angle divergence of the electrons have been shown in Fig. 2. Mean energy E_a is defined as the average energy over all of the electrons within the leading edge of the pulse. Here θ_a is defined as the average divergence angle at a particular moment and $\tan\theta_a = \overline{|y - y_c|}/(\overline{x - x_0})$, where y represents the transverse coordinates of the electrons within the leading edge of the laser pulse and x represents the longitudinal coordinates of the electrons, $x_0 = 84.0127$ μm is the initial longitudinal coordinate of the electrons and y_c represents the center position between the upper and lower boundaries of the target foils. Figure 2(a) shows the entire acceleration process including three parts: (1) E_a increases rapidly during the period of $0 < \tau \leq 419$, where τ is normalized by laser frequency ω. The electrons are efficiently accelerated to GeV quickly in about 178 fs. (2) For the foils of $n_{e0} = 5n_c$ and $n_{e0} = 15n_c$, E_a increased slowly with time at $\tau > 419$ and finally reached $\sim$1.3 GeV($n_{e0} = 5n_c$) and $\sim$1.1 GeV($n_{e0} = 15n_c$) at

$\tau = 2000$, respectively. During the whole process, the electrons are accelerated sequentially with time and continue to gain energy slowly in $\tau > 2000$. (3) For the foils of $n_{e0} = 25n_c$ and $n_{e0} = 30n_c$, E_a finally tends to constants after they reached their maximums, respectively. To sum up, electrons with the initial density $n_{e0} = 5n_c$ can be accelerated efficiently and gain about 1.3 GeV energy while electrons with the higher initial density ($n_{e0} = 30n_c$) gain the lower energy at about 660 MeV. Note that the acceleration time decreases and the acceleration efficiency becomes worse with the increase in the electron density. The reason is as follows: with the increase in the electron density, the effect of the transverse expansion, plasma instability such as Coulomb interaction becomes increasingly significant and makes the electron layer break earlier. On the other hand, the higher density brings about more electrons that can be accelerated so that the average energy decreases and the trapped charge increases.

Due to the limitation of 2D simulation, the accurate charge value of the electrons cannot be obtained. Instead of the accurate value, a simple estimation can be performed to obtain the rough value. To minimize errors, one may assume that the shape of target foils is like a 'pie' in the 3D case. The diameter and thickness of the target foils are 2 μm and 10 nm, respectively. Total charges of the case $n_{e0} = 5n_c$ foil and the case $n_{e0} = 25n_c$ are about 44 pC and 220 pC, respectively. Therefore, according to the simulation results, assuming that half of the total electrons were accelerated, charges of the accelerated electrons are 22 pC and 110 pC (the quantity of actually accelerated electrons might be more than half due to the fact that nearly no electron goes backward), respectively.

Inspired from the theory model in Ref. [31], we have fitted the data points of the case $n_{e0} = 5n_c$ (the black dashed line in Fig. 2(a)) and the case $n_{e0} = 15n_c$ (the red dashed line in Fig. 2(a)) with the model

$$E_a = a\tau^b, \tag{1}$$

where a and b are constants. As shown by the dashed lines in Fig. 2(a),

$$E_a\ (\text{MeV}) \approx 165.5887\tau^{0.28},\ n_{e0} = 5n_c, \tag{2}$$

$$E_a\ (\text{MeV}) \approx 153.707\tau^{0.25},\ n_{e0} = 15n_c. \tag{3}$$

In the period of $\tau > 209$, the model and the simulation data are in relatively good agreement with each other, R-square values of the two fitting curves are 0.96231 ($n_{e0} = 5n_c$) and 0.93139 ($n_{e0} = 25n_c$).

The average angle divergence as a function of time during the acceleration process is shown in Fig. 2(b). One can see that the average divergence angle θ_a experiences a steep decline from $\theta_a \approx 3.5°$ to $\theta_a \approx 0.5°$ during $0 < \tau \leq 200$. Then θ_a tend to be constants ($\sim$0.5° for the case $n_{e0} = 5n_c$ and $\sim$0.25° for the case $n_{e0} = 25n_c$) in $\tau > 200$. This is due to the fact that most of the laser pulse energy contributes to increasing the acceleration length due to the ponderomotive force $F_p = -m_e c^2 \nabla\gamma$ or radiation pressure and the electrons are accelerated to high energy quickly and have large relativistic masses, which overcomes their space charge forces significantly. On the whole, electron beams with a slight divergence angle can be obtained.

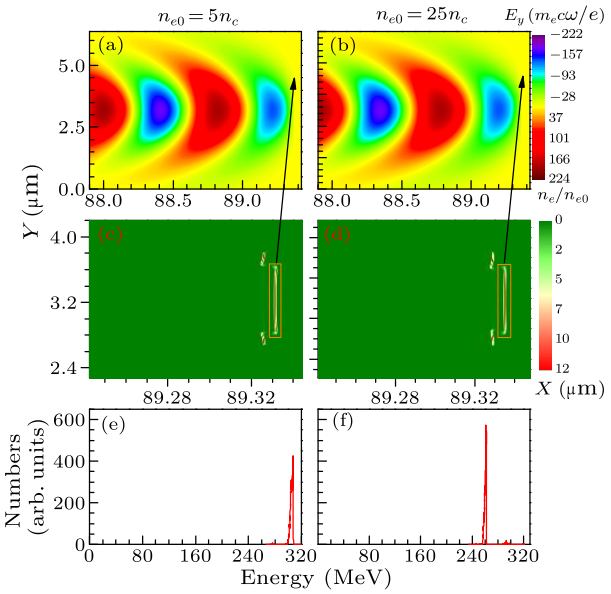


Fig. 3. (Color online) Simulation results by 2D OSIRIS at $t = 17.8$ fs: at the beginning, electrons are pushed forward and gain a very high accelerating gradient, where E_y is the normalized electric field of the laser pulse, X and Y are the longitudinal coordinate and the transverse coordinate respectively, n_{e0} is the initial density of the electrons. [(a), (b)] The space distribution of the laser pulse electric field strength. [(c), (d)] The density distribution of the electrons in the x–y plane. Electrons in the orange circle are efficiently accelerated. [(e), (f)] The distribution of the electron number as a function of electron energy.

For the purpose of performing the acceleration process in detail, the density distribution of the electrons, the space distribution of the amplitude of the laser pulse electric field and the electron energy spectrum have been shown in Figs. 3–5 at three different moments for the foils of $n_{e0} = 5n_c$ and $n_{e0} = 25n_c$. Here the source foils are located at $x = 84.0127$ μm when $t = 0$. As shown in Figs. 3(c) and 3(d), at the beginning ($t = 17.8$ fs), when the laser pulse interacts with the source foil, the electrons are compressed to high density and pushed forward to be separated from the ions as a whole.[25] Electrons in the laser leading edge (in the orange circle) are accelerated efficiently and continuously. This forms an electron layer which is opaque for the laser pulse as shown in Figs. 3(a) and 3(b). Here $E_y = m_e c\omega/e$ is the normalized electric field of the laser pulse. The laser pulse is reflected and forms a strong electric field behind the electron layer. The average energy of the electrons reaches up to $\sim$300 MeV (FWHM: 1.89 MeV) for $n_{e0} = 5n_c$ and $\sim$260 MeV(FWHM: 1.638 MeV) for $n_{e0} = 25n_c$ with energy spread of $\sim$0.63% respectively. Note that the acceleration length is only about 5.34 μm and the bunch width is only about 0.001μm.

As shown in Figs. 3(c) and 3(d), ultra-thin ($\sim$0.5 nm for the case $n_{e0} = 25n_c$) electron layers

appear (in the orange rectangles). The vast majority of the electrons are included and gain relativistic energy. The ultra-thin thickness, ultra-intense laser pulse and high initial density lead to the high compression rate of $n_{\rm e} \approx 60n_{\rm c} \approx 12n_{\rm e0}$ for $n_{\rm e0} = 5n_{\rm c}$ and $n_{\rm e} \approx 300n_{\rm c} \approx 12n_{\rm e0}$ for $n_{\rm e0} = 25n_{\rm c}$ at this moment. The relativistic electron mirror,[24,25] which is very difficult to form in the laser-wakefield acceleration mechanism, appears.

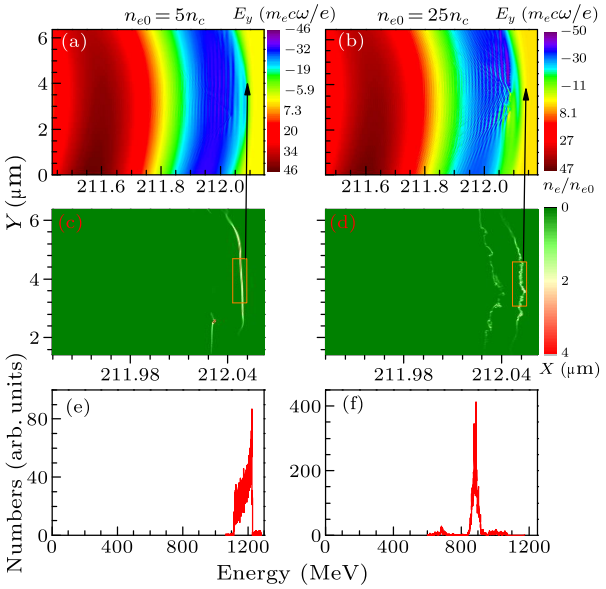


Fig. 4. (Color online) Simulation results by 2D OSIRIS at $t = 426.94$ fs: it is in a gentle acceleration period and transverse expansion appears. Definitions of the small Figs. (a)–(f) are the same as those in Fig. 3.

According to Ref. [24], the forces acting on the REM can be described by

$$F_{x\rm L} = 2\pi\sigma e(1+\beta_x)^{-1}\beta_y^2, \tag{4}$$

$$F_{x\rm R} = -2\pi\sigma e(1-\beta_x)^{-1}\beta_y^2, \tag{5}$$

where $F_{x\rm L}$ and $F_{x\rm R}$ are the radiation-reaction forces acting on the REM electrons at the leftmost and rightmost respectively, and σ is the surface density, $\beta_x = V_x/c$ and $\beta_y = V_y/c$. Here V_x and V_y are the electron velocities along the x-direction and y-direction, respectively. Note that $F_{x\rm L}$ and $F_{x\rm R}$ have opposite signs, thereby indicating the high compression of the electron bunch with large a_0. These forces slow down the electrons with velocities larger than the mean velocity of the layer and accelerate the delaying ones and this can partially prevent the expansion of the REM. The forces are just like magnetic attractive forces between the parallel currents of moving charges. Actually, the electrons with the same x-coordinates move transversely due to the laser pulse field and form an electric current. If the movement of the electrons is synchronous then these currents attract each other. As discussed above, the flying mirror can be used in the production of x-ray or γ-ray by Thomson backscattering,[6,29] in free-electron lasers for injection, and in many other applications. Note that the electron layer can maintain its shape for hundreds of femtosecond as shown in Figs. 4(c) and 5(c).

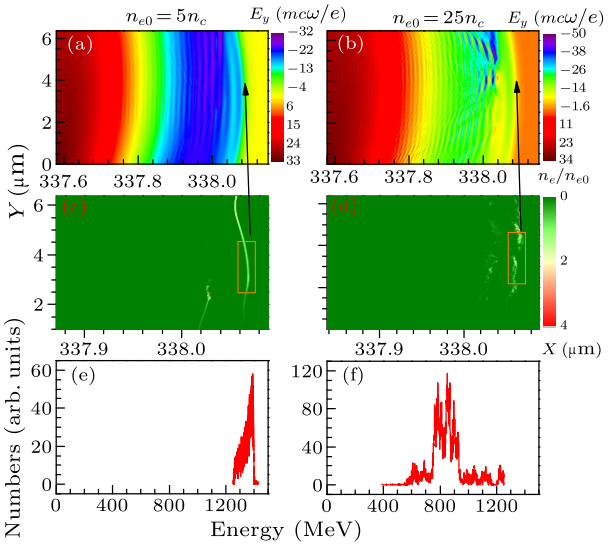


Fig. 5. (Color online) Simulation results by 2D OSIRIS at $t = 846.8$ fs: the electric field is distorted evidently at the leading edge of the laser pulse. Transverse expansion and plasma instability are significant and energy spread increases. An ∼1.3 GeV electron beam with the energy spread of 2.2% is obtained. Definitions of the small Figs. (a)–(f) are the same as those in Fig. 3.

Figure 4 shows that after several hundreds of femtosecond ($t = 426.94$ fs), electrons gradually leak out from the electron layer. The leaked-out ones move more slowly than the electrons in the front (in the orange circle), as shown in Figs. 4(c) and 4(d). The electron layers both have a lateral extension length of about 4 μm while only 0.8 μm at the beginning. Here E_y also extends to the whole space while its strength decreases. Therefore, the gentle acceleration period appears due to the transverse expansion and the decreased laser pulse intensity as shown in Fig. 2. The average energy of the electrons reaches up to 1.2 GeV(FWHM: 20.4 MeV) for $n_{\rm e0} = 5n_{\rm c}$ and 0.88 GeV(FWHM: 14.96 MeV) for $n_{\rm e0} = 25n_{\rm c}$ with the energy spread of ∼1.7%. At this moment, due to the more complex coulomb interaction, the source foil with the higher electron density induces a significant perturbation of E_y in the front of the laser pulse, as shown in Fig. 4(b). Densities of the electron layers ($n_{\rm e} \sim 2n_{\rm e0}$) are still above the critical density $n_{\rm c}$ making the layers remain opaque.

At $t = 846.8$ fs, as shown in Fig. 5, the intensity of the laser pulse attenuates further and the influence of the self-action of the electrons is significant. The energy spread increases, especially for the higher initial density foil in Figs. 5(b) and 5(d). The electron layer collapses and a hot electron cloud forms with a bunch width of roughly 0.1 μm. A small part of the laser pulse can penetrate through the middle region of the electron cloud. The chaotic distribution of the electrons nearly ends the acceleration with the energy spread up to ∼9% (shown in Fig. 5(f)). On the other hand, for the lower density foil, due to the weaker ex-

pansion, the electron layer ($n_e \sim 2n_{e0}$) still maintains its shape substantially and continues to gain energy slowly as shown in Figs. 5(a) and 5(c). A ~1.3 GeV (FWHM: 28.6 MeV) electron beam with the energy spread of ~2.2% is obtained after about 1 ps with the initial laser intensity of $a_0 = 223.5$ (Fig. 5(e)). During the whole process, nearly no electron goes backward.

Quasi-monoenergetic proton beams with GeV energy can also be produced from nanothickness foils irradiated by circular-polarization laser pulses.[32] However, to establish this mechanism of proton acceleration, the parametric region $a_0 \sim \sigma_0 = \hat{n}_e\hat{l}_e$ or $a_0 < 2\pi\hat{n}_e\hat{l}_e$ should be satisfied so that the protons are synchronously accelerated with the electrons. If the laser field a_0 is larger than the maximum normalized charge separation field $\epsilon = 2\pi\hat{n}_e\hat{l}_e = 2\pi\sigma_0$, all electrons will be displaced, then the balance between the laser field and the charge separation field will collapse. In our parametric region $a_0 \geq 800\sigma_0 \gg \sigma_0$, the laser field a_0 is much larger than the charge separation field ϵ. Therefore, the balance between the laser field and the charge separation field cannot be established (it is too late to establish the balance), thus the protons cannot be pulled out by the electrons. With the rapid increase of the distance between the electrons and the ions, the charge separation field decays very quickly while the laser field a_0 is still large. From Fig. 5, one can see that the laser field is still large ($a_0 \sim 50 > \epsilon$) even at the end of the acceleration process. Therefore, due to the fact that the parametric region $a_0 \sim \sigma_0 = \hat{n}_e\hat{l}_e$ cannot be satisfied, only the electrons are accelerated to relativistic energy.

Here we used CP laser pulses due to the fact that for a CP pulse with the electrical field $E_l = E(x)[sin(\omega t)\hat{y} + cos(\omega t)\hat{z}]$, the ponderomotive force $F_p = -\frac{m_e c^2}{4}\nabla_x a_0^2(x)\hat{x}$ has no oscillating component.[33,34] In contrast, the ponderomotive force F_p of a linearly polarized pulse with the electrical field $E_l = E(x)sin(\omega t)\hat{y}$ has a $2\omega t$ oscillating component, thus the accelerated electrons would oscillate periodically leading to the collapse of the electron layer and an increase of the energy spread. Therefore, it is difficult to obtain quasi-monoenergetic electron beams and the acceleration process may come to an end earlier when a linearly polarized pulse with the same intensity is used. When a CP laser is incident on a thin foil, the electrons are pushed forward steadily by the ponderomotive force without the oscillation and quasi-monoenergetic electron beams can be obtained easily.

In conclusion, we have demonstrated that high energy quasi-monoenergetic electron beams are generated efficiently in the parametric region $a_0 \geq 800\sigma_0$ by two-dimensional PIC simulation. Simulations show that GeV electron beams can be produced by the 10^{23} W/cm^2 CP laser pulse within a short time duration while the ions just move a very small distance compared with the accelerated electrons. The key in the new acceleration mechanism is to use a thin and relatively low density foil so that the electrons are trapped easily and the plasma instability may reduce. In this acceleration region, the electrons are accelerated to high energy quickly and have large relativistic masses, which overcome their self-action significantly and keep the acceleration stable. The REM comes into being in the early period of the acceleration process. It is opaque for the laser pulse and can maintain its shape by optimizing the initial parameters. Note that the average energy of the electrons as a function of time follows the simple model of $E_a = a\tau^b$, which may be useful to predict the final energy. Moreover, it is worth pointing out that a lower intensity laser pulse can still drive this acceleration scheme. For example, a 600 MeV quasi-monoenergetic electron beam with an energy spread of 9% is predicted for $a_0 = 111, l_e = 10$ nm, $n_{e0} = 5n_c$ at $t = 444.73$ fs. To sum up, for the ultra-short ultra-intense laser pulses discussed in this study, this acceleration scheme may be a new choice for laser-plasma electron acceleration in the near future.

References

[1] DesRosiers C et al 2000 *Phys. Med. Biol.* **45** 1781
[2] Glinec Y et al 2006 *Med. Phys.* **33** 155
[3] Glinec Y et al 2005 *Phys. Rev. Lett.* **94** 025003
[4] Leemans P W et al 2003 *Phys. Rev. Lett.* **91** 074802
[5] Shen Y et al 2007 *Phys. Rev. Lett.* **99** 043901
[6] Esarey E, Ride K S and Sprangle P 1993 *Phys. Rev.* E **48** 3003
[7] Matlis H N et al 2006 *Nat. Phys.* **2** 749
[8] Kitagawa Y et al 2004 *Phys. Rev. Lett.* **92** 205002
[9] Lu W et al 2005 *Phys. Plasmas* **12** 063101
[10] Lu W et al 2007 *Phys. Rev. Spec. Top. Accel. Beams* **10** 061301
[11] Tochitsky S et al 2004 *Phys. Rev. Lett.* **92** 095004
[12] Lindberg R R et al 2004 *Phys. Rev. Lett.* **93** 055001
[13] Umstadter D et al 1995 *Phys. Rev.* E **51** 3484
[14] Liu S J et al 2011 *Phys. Rev. Lett.* **107** 035001
[15] Chambaret P J et al 2010 *Extreme Light Infrastruct.: Laser Architecture Major Challenges Proc. SPIE 7721, Solid State Lasers and Amplifiers IV and High-Power Lasers 77211D* (Brussels, Belgium 12 April 2010)
[16] Froula H D et al 2009 *Phys. Rev. Lett.* **103** 215006
[17] Ralph E J et al 2010 *Phys. Plasmas* **17** 056709
[18] Leemans P W et al 2006 *Nat. Phys.* **2** 696
[19] Nakamura K et al 2007 *Phys. Plasmas* **14** 056708
[20] Clayton E C et al 2010 *Phys. Rev. Lett.* **105** 105003
[21] Schwoerer H et al 2006 *Nature* **439** 445
[22] Esirkepov T Zh et al 2004 *Phys. Rev. Lett.* **92** 175003
[23] Wang M W et al 2010 *Phys. Rev. Spec. Top. Accel. Beams* **13** 071301
[24] Kulagin V V et al 2007 *Phys. Rev. Lett.* **99** 124801
[25] Kulagin V V et al 2004 *Phys. Plasmas* **11** 5239
[26] Wang X et al 2006 *Phys. Plasmas* **13** 080702
[27] Chen L M et al 2008 *Phys. Rev. Lett.* **100** 045004
[28] Mordovanakis G A et al 2009 *Phys. Rev. Lett.* **103** 235001
[29] Wen M et al 2012 *Appl. Phys. Lett.* **101** 021102
[30] Hemker G R 2000 PhD Dissertation (Los Angeles: University of California)
[31] Esirkepov T et al 2004 *Phys. Rev. Lett.* **92** 175003
[32] Yan X Q et al 2008 *Phys. Rev. Lett.* **100** 135003
[33] Landau D L and Lifshitz M E 1980 *The Classical Theory of Fields* (Oxford: Pergamon Press)
[34] Pauli W 1981 *Theory of Relativity* (New York: Dover)